Preprints (www.preprints.org) | NOT PEER-REVIEWED | Posted: 9 May 2023 doi:10.20944/preprints202305.0617.v1

Disclaimer/Publisher's Note: The statements, opinions, and data contained in all publications are solely those of the individual author(s) and contributor(s) and not of MDPI and/or the editor(s). MDPI and/or the editor(s) disclaim responsibility for any injury to people or property resulting from any ideas, methods, instructions, or products referred to in the content.

Article

Methane dry reforming catalysts based on Pr-doped ceria-zirconia synthesized in supercritical propanol

Marina Arapova [1], Ekaterina Smal [1], Yuliya Bespalko[1], Konstantin Valeev [1], Valeria Fedorova [1], Amir Hassan [2], Olga Bulavchenko [1], Vladislav Sadykov [1,*] and Mikhail Simonov [1]

[1] Department of Heterogeneous Catalysis, Federal Research Center, Boreskov Institute of Catalysis, Lavrentiev Ave. 5, 630090 Novosibirsk, Russia

[2] Novosibirsk State University, 630090, Novosibirsk, Russia

* Correspondence: sadykov@catalysis.ru

Abstract: This work is devoted to the study of active and stable nickel catalysts for methane dry reforming based on Pr-doped ceria-zirconia obtained by solvothermal continuous method. The studies of physicochemical and catalytic properties of the 5%Ni\\$Ce_{0.75}Zr_{0.25-x}Pr_xO_2$ series showed that Pr introduction leads to an increase in the amount of highly reactive oxygen of the oxide lattice. Praseodymium-based catalysts showed significantly higher reactant conversions. In addition to the nature of support, the method of nickel introduction was also studied - Ni was added both by impregnation and one-pot with mixed oxide preparation. The method of Ni addition was shown to have significant effect on the morphology of the supported active component and, respectively, on the catalytic activity. The 5%Ni/$Ce_{0.75}Zr_{0.15}Pr_{0.1}O_2$ catalyst prepared by one-pot method showed stable operation in the MDR reaction for 30 hours at CO_2 and CH_4 conversions of ~40% and an H_2 yield of ~18% (T=700°C, τ=10ms).

Keywords: dry reforming; methane; ceria-zirconia; supercritical synthesis; oxygen vacancies; stability.

1. Introduction

Methane dry reforming (MDR) is a promising way to utilize two greenhouse gases - CH_4 and CO_2 - to convert them into synthesis gas with its subsequent use as a feedstock for the chemical industry or a fuel [1, 2, 3]:

$CH_4 + CO_2 = 2CO + 2H_2$, $\Delta H^0_{298} = 247.3$ kJ/mole (1)

In addition to direct use, it can be effectively integrated into existing hydrogen production chains, taking into account current environmental requirements [4]. MDR catalysts are representatives of typical catalysts for hydrocarbons reforming processes, which are a transition metal, primarily nickel, deposited on an oxide support [5]. Studies over the past decades show that the poor stability due to sintering and carbonization of the active species remains a major problem for the reforming catalysts [6]. Developing a thermally stable catalyst with superior activity and enhanced resistance to carbon formation and metal sintering is among the major challenges faced by industries and researchers [7].

The carbonization problem begins at the stage of competition between simultaneously occurring routes of CH_x intermediates transformation on metal particles. If CH_x oxidation occurs rapidly, the formation of the desired CO is observed. But if the rate of CH_x formation is higher than its oxidation, carbon deposits grow. A well-known, highly efficient approach to increase the rate of the desired route is to involve the lattice oxygen of the support into the catalytic cycle [8]. Fuels transformation over catalysts with high oxygen reactivity occurs by the redox reaction mechanism. During the reaction, the substrate (CH_4, CO) is oxidized by the lattice oxygen, accompanied by the formation of a vacancy and its replenishment through the activation of the oxidizer (CO_2, H_2O or O_2) on the oxide surface cations and its fast surface transfer to the direct catalytic act zone (reverse oxygen spillover) [9, 10].

© 2023 by the author(s). Distributed under a Creative Commons CC BY license.

Preprints (www.preprints.org) | NOT PEER-REVIEWED | Posted: 9 May 2023 doi:10.20944/preprints202305.0617.v1

However, establishing an unambiguous relationship between the structural characteristics of the oxide and the catalytic activity in reforming reactions is still a debatable issue: steady-state reaction conditions are differed from equilibrium, while the properties of as-prepared catalysts are more likely defined by thermodynamic equilibrium during the preparation process [11]. Nevertheless, huge number of works has been done and described in the literature based on a complex of catalytic, structural studies and DFT calculations, which showed correlations of catalytic activity with the so-called «support oxygen activity» [7, 12, 13].

The term "support oxygen activity" is complex, including several correlated characteristics of the oxide's lattice oxygen, such as oxygen storage capacity (OSC), surface and bulk mobility, the number and formation energy of oxygen vacancies. For example, according to many reports, the redox properties of catalysts were believed to relate to the amount of oxygen vacancies (regarded as active sites) in oxide catalysts. However, just presence of vacancies is not enough: if the vacancy formation barrier is too high, this stage becomes rate-limiting, which casts doubt on the probability of the entire process proceeding along such a route. That phenomenon, for example, was shown and confirmed by DFT calculations for nickel-containing undoped cerium oxide [14]. Moreover, the steady-state concentration of oxygen vacancies is related to the rates of vacancy formation and vanishing. In other words, a real active oxygen vacancy should have a high abilities of adsorbing the reactant molecules and desorbing the product molecules [11, 15]. A decrease in the energy of vacancy formation can be achieved, for example, by increasing the length of at least one oxygen bond in the lattice, or by creating so-called asymmetric vacancies [16, 17].

Oxides capable of providing such cycles of lattice vacancies formation with charge compensation due to a cation with a variable valence are mainly transition-metal oxides and are called reducible, or oxides with the active oxygen [18]. Among oxides with the lattice oxygen taking part in the reaction, the most common are perovskites, spinels and fluorites. The group of oxides based on ceria doped with a wide range of cations is deeply studied [12, 19- 21]. Detailed kinetic and computational studies have shown that the activity of oxygen in such oxides depends on the concentration and formation energy of these vacancies [22, 23]. Moreover, it was also shown that the presence and energy of the vacancies on the surface of cerium oxide can determine the overoxidation of the surface intermediate -CO into -CO_2, thus largely determining the H_2/CO ratio in the resulting synthesis gas [24, 25]. One of the most popular doping cations which also increases thermal stability of CeO_2 oxide is Zr [26, 27]. The effective generation of asymmetric vacancies in the CeO_2-based oxides upon doping with Pr increasing the oxygen catalytic activity has been shown in a number of works [14, 28, 29, 30]. Furthermore, substitution of no more than 25% of cerium has been shown to be effective, since the Pr extent would hamper the Ce^{4+}/Ce^{3+} redox pair by exclusively locating electrons generated by the vacancy formation at praseodymium centers and prevent completion of the catalytic cycle [16, 18].

The synthesis method of these polycation oxides for catalytic application should provide a high chemical uniformity and oxide dispersion. Known to use methods are: coprecipitation [31], hydrothermal method [32], solvothermal method [33], sol–gel–citrate [34, 35] and ester polymer precursors (Pechini) [36], microemulsions [37], microwave method [38, 39], sonochemical method [40], solution combustion [41, 42], spray pyrolysis reactions [43]. The use of the solvothermal method for the synthesis of such polycationic oxides provides structural homogeneity, as well as improved textural characteristics and tunable particle size distribution [44].

It is important to emphasize the decisive influence of the nickel introduction method. In an oxide-metal system, the dispersion of the supported metallic particles and the strength of its interaction with the support are the key properties that determine catalyst stability in reforming reactions on a par with the support oxygen activity [45, 46, 47]. It was shown that the traditional method of wet impregnation is less efficient than the method of nickel introducing into the oxide structure at the stage of support synthesis. In the second case, during the reduction pretreatment, formation of finely dispersed metal particles strongly bound to the carrier is observed [48, 49]. At the same time, the main disadvantage of this method is the possible loss of the active component in the volume of the support blocked for the reaction.

Hence, the use of zirconium as a doping cation to ceria increases stability of the structure and increases the structure defectiveness, while doping with praseodymium makes it possible to increase

Preprints (www.preprints.org) | NOT PEER-REVIEWED | Posted: 9 May 2023 doi:10.20944/preprints202305.0617.v1

the number of oxygen vacancies and obtain more reactive surface oxygen. Accordingly, in this work, our goal was the synthesis of a series of complex metal-oxide catalysts 5%Ni\$Ce_{0.75}Zr_{0.25-x}Pr_xO_2$ obtained by the solvothermal method with Ni added by both impregnation and one-pot method. This work present results of the study of 5%Ni\$Ce_{0.75}Zr_{0.25-x}Pr_xO_2$ textural and redox properties and their influence on the catalytic performance in the MDR reaction.

2. Materials and Methods

2.1. Synthesis methods

The catalyst supports were synthesized in supercritical alcohol media using original installation shown in the Figure 1. Cerium nitrate $Ce(NO_3)_3 \cdot 6H_2O$ (Vekton, Russia), praseodymium nitrate $Pr(NO_3)_3 \cdot 6H_2O$ and zirconium butoxide (80 wt% in n-butanol, Alfa Aesar, Germany) were dissolved in required proportions in isopropanol (Reakhim, Russia). Then the solution was fed into the reactor and synthesis was carried out according to the method described earlier [50]. For impregnated catalysts, nickel was supported by the incipient wetness impregnation of supports with water solution of $Ni(NO_3)_2$ [49].

For one-pot catalysts, nickel nitrate $Ni(NO_3)_2 \cdot 6H_2O$ (Vecton) was dissolved together with Ce, Zr (Pr) salts, and synthesis in a supercritical medium was carried out according to the procedure described above. All catalysts were dried at 200°C and calcined at 700°C for 2 h. The loading amount of Ni was 5 wt% both for impregnated and one-pot catalysts. The abbreviations of the prepared samples are presented in the Table 1.

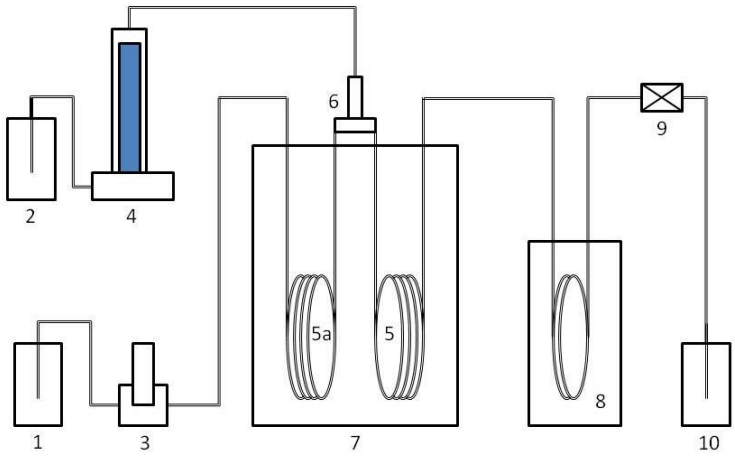

Figure 1. Experimental setup for solvothermal continuous synthesis. 1 – vessel with isopropanol, 2 – vessel with a solution of metal salts, 3 – plunger pump, 4 – syringe pump, 5 – reactor, 5a – isopropanol pre-heater, 6 – mixer, 7 – oven, 8 – heat exchanger, 9 – back pressure valve, 10 – storage tank.

2.2. Characterizations

Specific surface area (SSA) was defined by the BET method using a Quadrasorb evo (Quantachrome Instruments, USA) installation. Pore volumes and pore size distribution were determined from the desorption branch of the isotherm using the BJH method.

XRD analysis was performed on a Thermo X'tra diffractometer, in the angle range of 20-85° with a step of $2\theta = 0.02°$ and a speed of 1°/min, using a Mythen2R 1D linear detector (Decstris, Switzerland). The CuKα radiation ($\lambda = 1.5418$A) was used. The average sizes of coherent scattering regions (CSRs) were calculated using the Scherrer formula from the 111 fluorite reflection. The description of the diffraction profile was performed using the Fityk program with the Lorentz function.

Preprints (www.preprints.org) | NOT PEER-REVIEWED | Posted: 9 May 2023 doi:10.20944/preprints202305.0617.v1

XRD with H_2 *in situ* analysis was made on a Bruker D8 Advance diffractometer (Germany), in the angle range of 20-55° with a step of 2Θ = 0.05° and an accumulation time of 3 s at each point using a LynxEye (1D) line detector. The monochromatic CuKα radiation (λ = 1.5418Å) was used. The measurements were carried out using an XRK-900 high-temperature reactor chamber (Anton Paar, Austria). The 10%H_2/90%He mixture at a flow rate of 100 mL/min was passed through the chamber during heating and cooling to room temperature. Heating was carried out according to the following scheme: 250, 315, 400, 500, 700, 30°C with the heating rate 12°/min. Refinement of lattice parameters and phase relationships was performed by the Rietveld method [51]. In the refinement, the CeO_2 structure was used; only Ce atoms were in the cationic position.

TEM with EDX. TEM (transmission electron microscopy) micrographs were obtained with a Themis-Z 3.1 instrument (TFS, USA) equipped with X-FEG-monochromator and CS/S double corrector, accelerating voltage 200 kV, and with a JEM-2200FS transmission electron microscope (JEOL Ltd., Japan, acceleration voltage 200 kV, lattice resolution ~ 1 A) equipped with a Cs corrector. Elemental analysis was performed with a Super-X EDS detector (energy resolution about 120 eV) in HAADFSTEM mode. Samples for the TEM study were prepared by ultrasonic dispersing in ethanol and subsequent deposition of the suspension upon a "holey" carbon film supported on a copper grid.

TPR-H_2. Temperature-programmed reduction by hydrogen was carried out from 25 °C to 900°C in a flow installation with a Tsvet 500 (JSC Tsvet, Russia) thermal conductivity detector using 10 vol% H_2 in Ar feed at the flow rate 40 ml/min.

2.3. Catalytic Tests

The catalysts were preliminary reduced in a stream of 5% H_2 in He at 600 ◦C for 1 hour. The catalytic activity in methane dry reforming reaction was studied using a tubular quartz plug flow reactor and gas analyzer with IR sensors for CO, CO_2 and CH_4, and electrochemical sensor for H_2 (Boner LLC, Novosibirsk, Russia). Studies were conducted with the initial mixture of 15% CH_4 + 15% CO_2 + 70 % N_2 in the temperature range of 600–750 ◦C and contact time 10 ms. Long-term stability tests were carried out for 30h at 700 ◦C.

3. Results

3.1. Textural and structural features

Table 1 lists designation, chemical composition and specific surface area (SSA) of samples obtained.

Table 1. Sample's designation, composition, synthesis methods, SSA and F_{m3m} lattice parameter.

Designation	Ni addition method	Composition	SSA, m^2/g	a, Å
CZP	-	$Ce_{0.75}Zr_{0.15}Pr_{0.1}O_2$	14	5.403(1)
N/CZP	impregnation	5%Ni/$Ce_{0.75}Zr_{0.15}Pr_{0.1}O_2$	9	5.397(1)
N+CZP	one-pot	5%Ni+$Ce_{0.75}Zr_{0.15}Pr_{0.1}O_2$	14	5.407(1)
CZ	-	$Ce_{0.75}Zr_{0.25}O_2$	29	5.369(1)
N/CZ	impregnation	5%Ni/$Ce_{0.75}Zr_{0.25}O_2$	21	5.373(1)
N+CZ	one-pot	5%Ni+$Ce_{0.75}Zr_{0.25}O_2$	14	5.372(1)

As can be seen, samples obtained do not have a very high specific surface area: the values of SSA for the entire series of samples are about 10-30 m^2/g. The introduction of praseodymium reduces the specific surface area of the initial support from 29 m^2/g for CZ to 14 m^2/g for CZP. It correlates well with the data of pore's size distribution (Fig. 2), where the number of micropores for praseodymium-

Preprints (www.preprints.org) | NOT PEER-REVIEWED | Posted: 9 May 2023 doi:10.20944/preprints202305.0617.v1

doped samples is significantly reduced. In contrast, for samples prepared by the one-pot method (N+CZ and N+CZP) there is no difference in the SSA values.

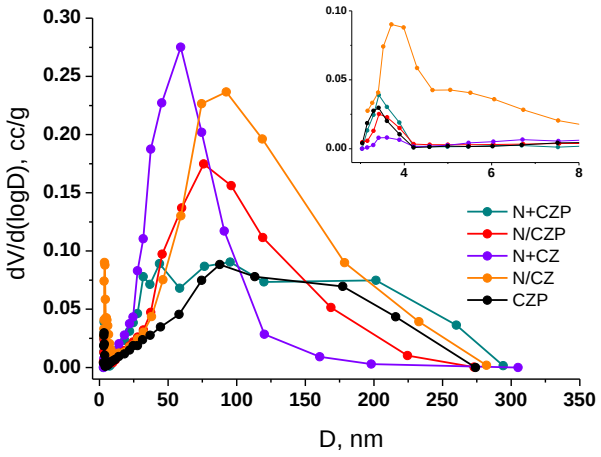

Figure 2. The pore size distribution for the supports and Ni-containing samples.

According to XRD data (Fig. 3), for the entire series main intense peaks located at 2θ = 28.7, 47.7, 56.6, 59.4, 69.8, 77.0, 79.4º correspond to 111, 200, 220, 311, 222, 331, 420, 422 reflections of the fluorite structure F_{m3m} (PDF 81-0792). There are no reflections of Zr and Pr individual oxides for all series. For Pr-containing samples, the absence of double peaks and a shift of the fluorite peaks to the lower angles' region (Fig. 2, Table 1) suggest that praseodymium is embedded into the CZ cubic structure, which is consistent with literature data [1, 2]. The ability of praseodymium to replace cerium without destroying the fluorite structure is ensured by close radii of cations of the same valencies (Ce^{4+} = 1.110 Å; Pr^{4+} = 1.100 Å; Ce^{3+} = 1.283 Å; Pr^{3+} = 1.266 Å), and a slightly higher Pr^{4+}/Pr^{3+} redox potential leads to the formation of a structure with more active oxygen compared to undoped ones [52, 54].

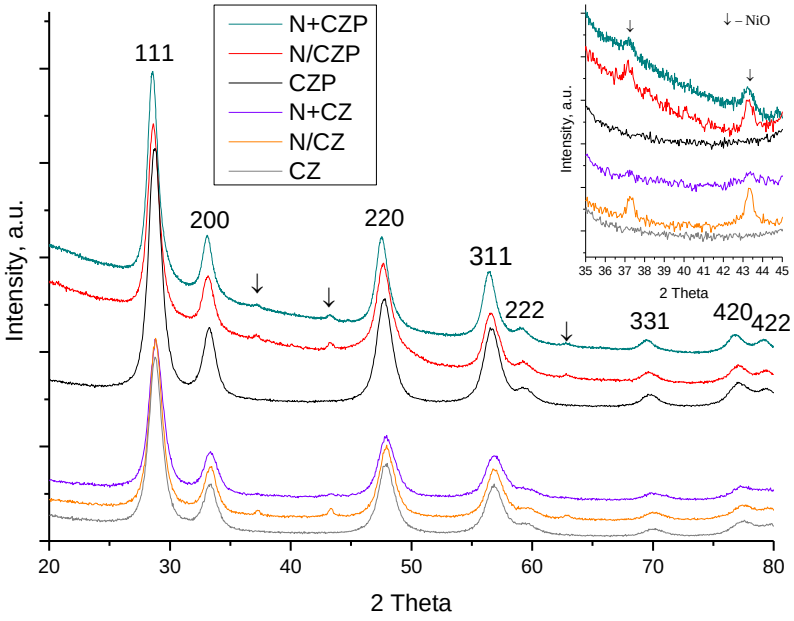

Figure 3. Diffraction pattern of supports and Ni-containing samples. Reflections of the fluorite structure are marked by (hkl) indices, the arrows indicate the NiO reflections.

Preprints (www.preprints.org) | NOT PEER-REVIEWED | Posted: 9 May 2023 doi:10.20944/preprints202305.0617.v1

The method of the nickel introducing has a strong effect on the oxide's morphology. XRD (Fig. 3) and TEM data (Fig. 4) show that the deposition of nickel by wet impregnation on the formed oxide resulted in the formation of large well-crystallized NiO particles about 20 nm in size, weakly bound to the support. For this samples, there are peaks at 2θ = 37.4, 43.3, 62.8 º, which can be associated with 111, 200 and 220 reflections of nickel oxide NiO (F_{m3m}). The introduction of nickel at the stage of support synthesis leads to the incorporation of a significant amount of nickel into the fluorite structure and formation of residual finely dispersed NiO particles firmly fixed on the oxide surface or encapsulated into it.

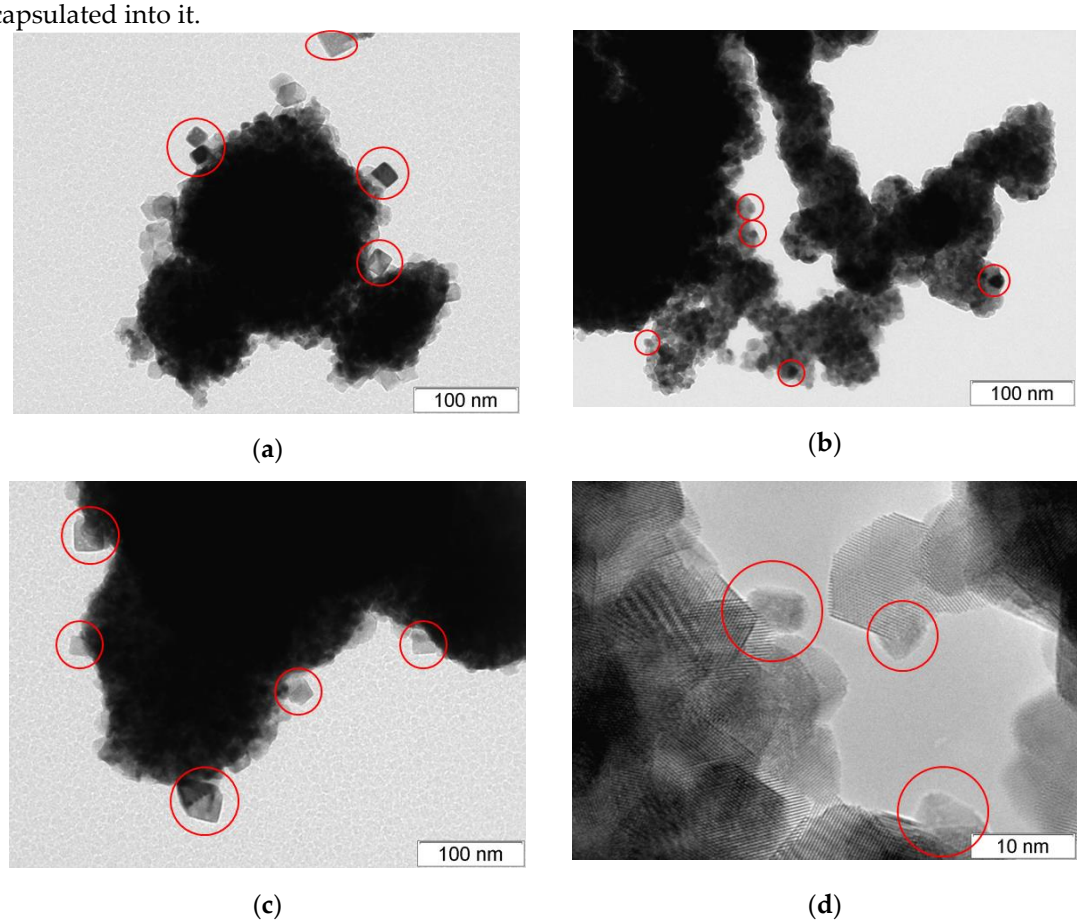

(**a**) (**b**)

(**c**) (**d**)

Figure 4. TEM: (**a, c**) impregnated Ni/CZP; (**b, d**) one-pot N+CZP.

3.2. Reducibility and oxygen reactivity

The oxide's oxygen activity was estimated by a combination of complementary methods – TPR-H_2 and XRD with *in situ* H_2-reduction. The TPR-H_2 results are presented in the Figure 5. The curves of two supports (CZ and CZP) represent two reduction regions, classical for these oxides: the medium-temperature one, related to the reduction of the more reactive surface oxygen, and the high-temperature reduction of bulk oxygen, limited by the internal diffusion. It can be seen that for the support with praseodymium, both the start of reduction and the maximum of the first peak are shifted by about 200 °C towards lower temperatures, which indicates a significant facilitation of the reduction of surface oxygen with doping.

Preprints (www.preprints.org) | NOT PEER-REVIEWED | Posted: 9 May 2023 doi:10.20944/preprints202305.0617.v1

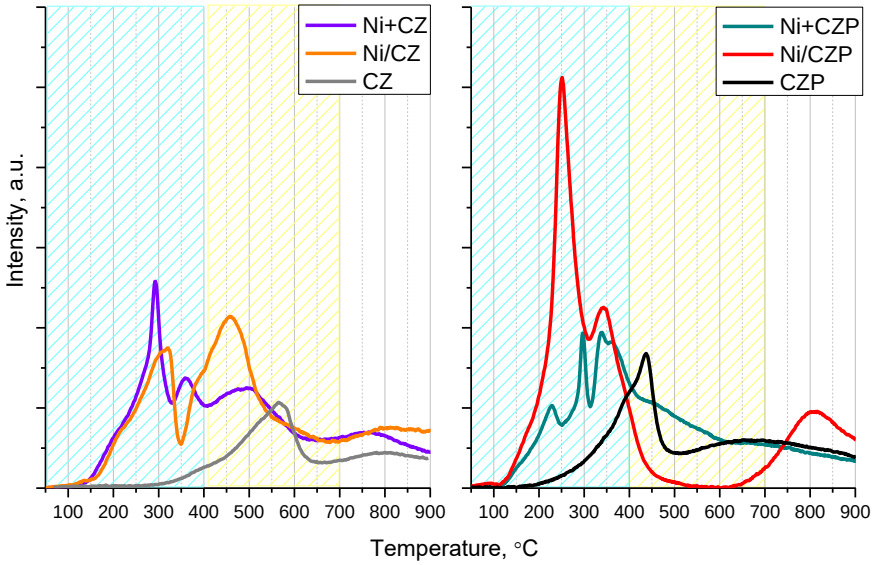

Figure 5. TPR-H_2 patterns for the supports and Ni-containing samples.

All curves of Ni-containing samples have a complex contour with peaks that are difficult to separate from each other. The calculation of the total amount of hydrogen consumed over the entire temperature range shows approximately the same values for all samples: 2.0–2.15 mmol/g_{cat}. However, significant changes in the nature of reduction are noted with the introduction of praseodymium and nickel to CZ. For the supported N/CZP, a large sharp peak is observed with a maximum at 250 °C, which corresponds to the reduction of significant amount of NiO and indicates its weak interaction with the oxide support. For the one-pot N+CZP sample, the reduction occurs more uniformly in the range of 200-400 °C. The XRD with *in situ* H_2 reduction (Fig. 6, a-c) confirms that, after reduction at 400 °C, a significant amount of metallic nickel (2θ=44.2 °) is detected for all nickel-containing samples. Moreover, in the temperature range of 400–500 °C, the intensity of nickel reflections for supported catalysts is higher compared to one-pot samples, which is consistent with the TPR-H_2 data and the assumption that nickel is partially incorporated into the fluorite lattice in one-pot samples.

The XRD with *in situ* H_2 reduction shows also (Fig. 6, d) non-linear change in the lattice parameter in the temperature range of 200–400 °C, where hydrogen interaction with the most reactive oxide's oxygen occurs. Stronger parameter changes in this region for Pr-containing catalysts compared to undoped ones confirms facilitation of the lattice oxygen release obtained by the TPR-H_2 method with Pr doping. A noticeable overstating value of the lattice parameter at 300-400 °C coincides with the appearance of the nickel metallic reflections on the XRD patterns and indicates a greater depth of reduction due to a well-known phenomenon of hydrogen spillover described in the literature [55, 56, 57]. It is also important to note that after returning to the room temperature, the F_{m3m} fluorite monophase with an increased parameter is preserved, hence, the release of oxygen occurs without destroying the structure.

Preprints (www.preprints.org) | NOT PEER-REVIEWED | Posted: 9 May 2023 doi:10.20944/preprints202305.0617.v1

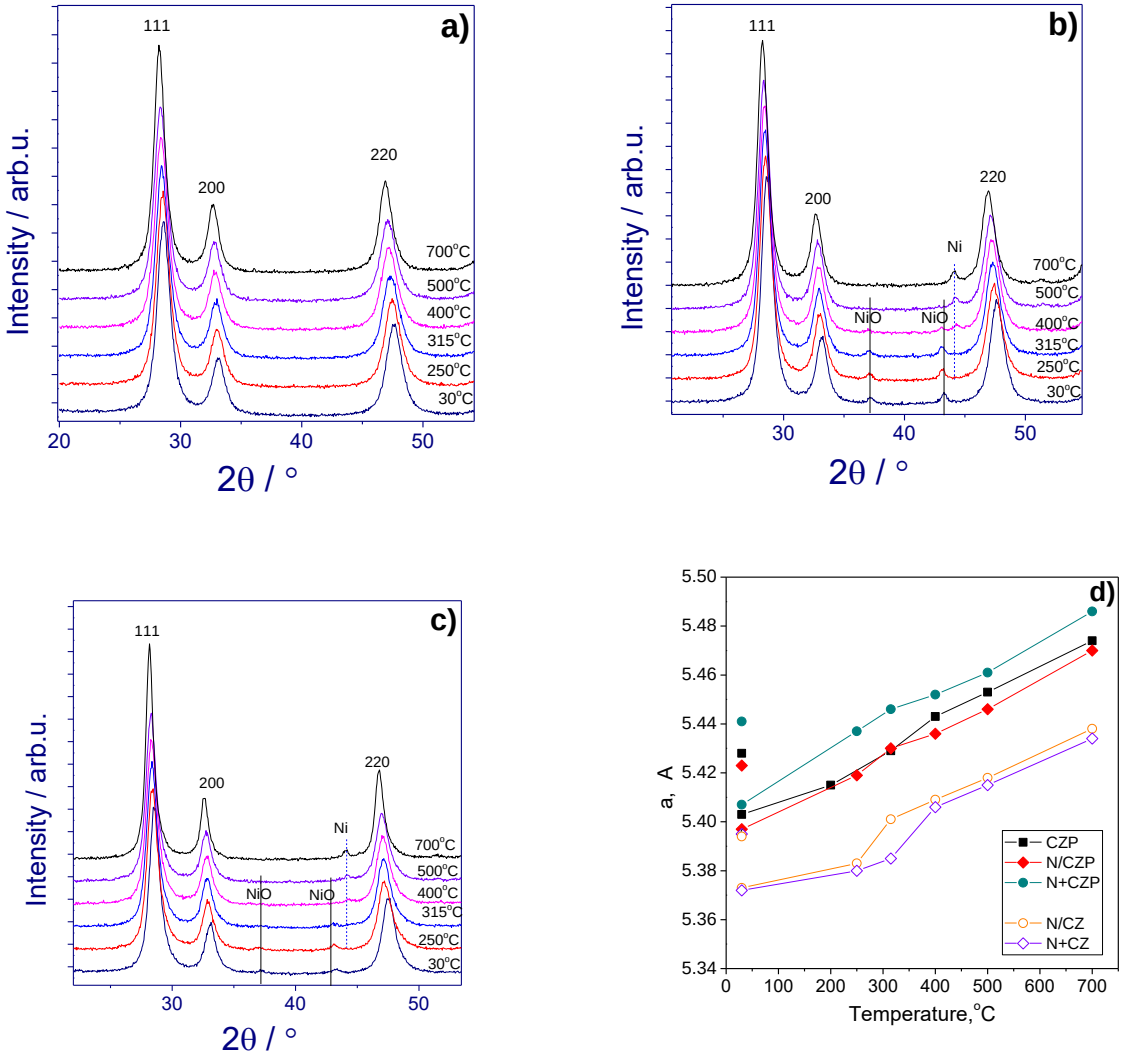

Figure 6. Diffraction patterns recorded during *in situ* reduction: (**a**) CZP; (**b**) N/CZP; (**c**) N+CZP. The reflections of the fluorite structure are labeled; the positions of the NiO peaks are indicated by solid lines, and Ni by dotted lines. (d) Fluorite lattice parameters versus temperature.

3.3. Catalytic activity in MDR

The results of MDR catalytic experiments are shown in Figure 7. For all samples, an increase in the conversions of methane and carbon dioxide is observed with increasing temperature in accordance with the endothermicity of the reaction.

The activity of Pr-containing catalysts N/CZP and N+CZP exceeds the activity of samples based on undoped CZ support, and the difference rises significantly with the temperature increasing. This is consistent with literature data describing increase in the contribution of support to the reaction with the temperature rise due to more efficient activation of CO_2 and transfer of active oxygen forms over the oxide surface to the metal-support interface [24, 25].

Preprints (www.preprints.org) | NOT PEER-REVIEWED | Posted: 9 May 2023 doi:10.20944/preprints202305.0617.v1

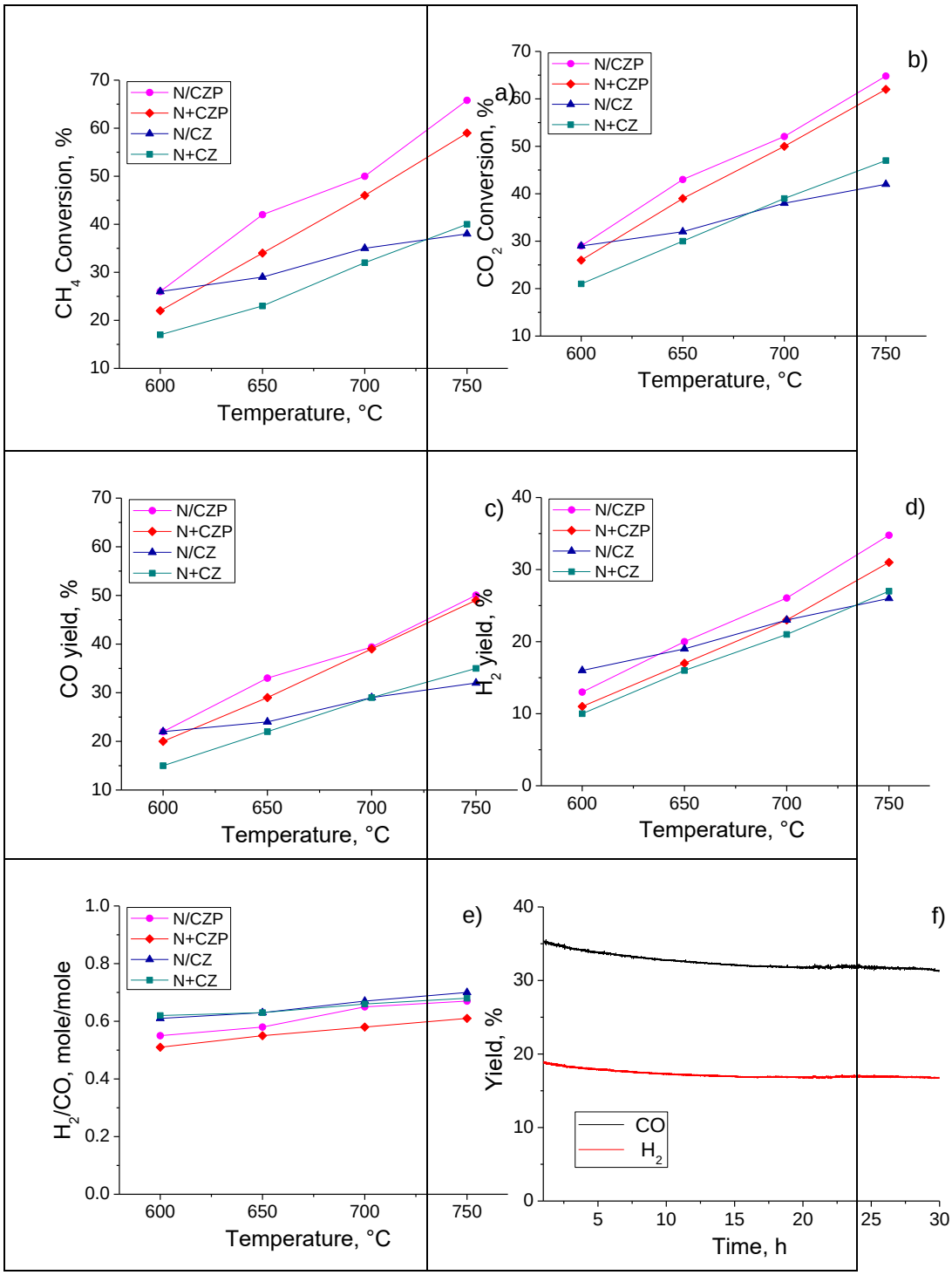

Figure 7. Results of catalytic tests for the N/CZ(P) and N+CZ(P) catalysts in methane dry reforming: temperature dependences of a) CH_4 conversion b) CO_2 conversion; c) CO yield, d) H_2 yield, e) H_2/CO; and f) H_2 and CO yields in long-term tests for N+CZP one-pot catalyst at 700 °C. Catalyst grain size 0.25-0.5 mm, contact time 10 ms, $C^0(CH_4) = C^0(CO_2) = 15\%$.

At the same time, the method of nickel introduction does not noticeably affect the activity in experiments with temperature variation, but strikingly determines stability in long-term tests. For the N/CZP sample obtained by wet impregnation, reactor plugging due to carbon formation occurs within 1 hour of a long test at 700 °C (not shown on Figures). Figure 7, f, shows the data on the H_2 and CO yields in long-term tests for N+CZP one-pot catalyst. For 30 hours of the reaction, the hydrogen yield decreased from 35 to 32%, and the CO yield - from 19 to 17%, and the main drop occurred for the first 3 hours of reaction. Previously, for such systems, we have shown that this decrease in

Preprints (www.preprints.org) | NOT PEER-REVIEWED | Posted: 9 May 2023 doi:10.20944/preprints202305.0617.v1

first hours is associated with the rapid carbon formation, that comes to steady state with reaction of carbon oxidation after 3 hours of reaction and further the carbon formation rate (CFR) decreases almost linearly with increasing time [58].

The TEM studies of catalysts after reaction showed that the N/CZP sample is characterized by whiskers carbon deposits and weak bond between nickel and the support resulted in detachment of nickel particles from the surface, while the N+CZP sample demonstrates metal particles firmly fixed on the oxide surface and an insignificant number of thin layers of carbon directly on the metal particles that do not block active catalytic centers (Fig.8).

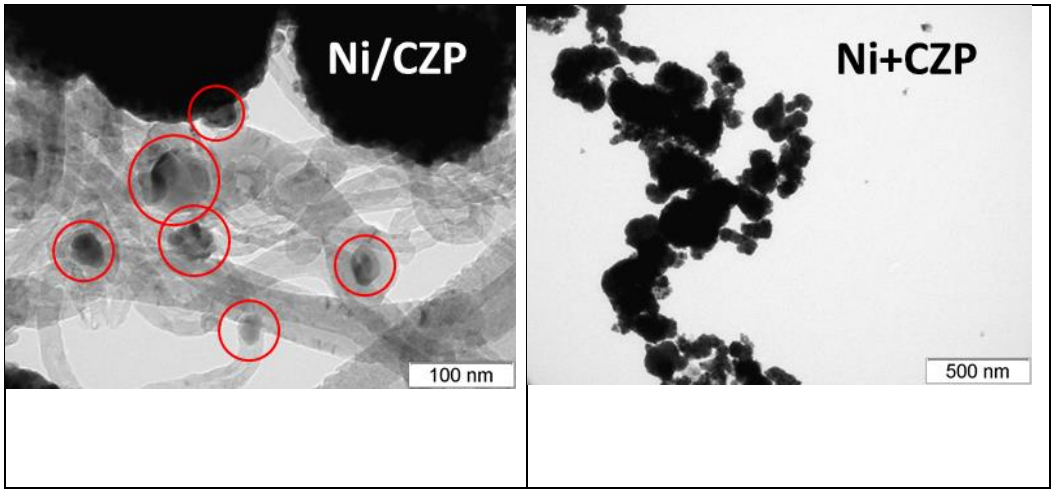

Figure 8. TEM of Ni/CZP and Ni+CZP catalysts after reaction. Nickel particles are marked with circles.

Hence, the catalytic activity of samples modified with praseodymium is significantly higher than that of the unmodified ones. An increase in the conversion of both methane and CO_2 correlates with an increase in the activity of the carrier's highly reactive oxygen, as shown by the TPR-H_2 method. At the same time, stability of the catalyst is dramatically affected by the strength of the interaction of resulting nickel metal particles with the oxide support. Thus, for samples obtained by wet impregnation, the weak bond with the support, shown by TEM and TPR-H_2 methods, eliminates all the advantages of the active support and prevents the effective occurrence of the redox mechanism, that leads to rapid deactivation with formation of a significant amount of fibrous carbon deposits, confirmed by TEM images. For samples with nickel introduced at the stage of support formation, high stability for 30 hours of reaction at 700°C and the absence of carbon deposits in TEM images were shown.

5. Conclusions

In this work, catalysts series 5%Ni\\$Ce_{0.75}Zr_{0.25-x}Pr_xO_2$ (x=0; 0.1) were successfully synthesized by the solvothermal method in a flow-through setup in supercritical isopropanol. It was shown that all samples are crystallized in the structural type F_{m3m} of cubic fluorite with the incorporation of praseodymium and zirconium cations into the lattice. Addition of Pr to mixed ceria-zirconia leads to increased reducibility during TPR-H_2 experiments and stronger parameter changes during *in situ* XRD in hydrogen which together confirm higher reactivity of lattice oxygen. The nickel introduction into the catalyst composition directly at the stage of support synthesis (one-pot) allows a significant amount of nickel to be incorporated into the fluorite structure, which leads both to an increase in the defectiveness of the oxide and to the formation of highly dispersed particles of metallic nickel, strongly bound to the support oxide, during reduction pretreatment. The Pr introduction into the oxide support significantly increases catalysts activity in syngas production, which is most likely associated with facilitating the oxidant molecule activation, thus promoting the redox mechanism of MDR. The use of Pr-doped ceria-zirconia as a support makes it possible to achieve excellent stability due to the high dispersion of metal particles, the optimal strength of the metal-support interaction,

Preprints (www.preprints.org) | NOT PEER-REVIEWED | Posted: 9 May 2023 doi:10.20944/preprints202305.0617.v1

and lattice oxygen activity in reactions of oxidant activation and gasification of carbon precursors. The 5%Ni/$Ce_{0.75}Zr_{0.15}Pr_{0.1}O_2$ catalyst showed stable performance in the MDR reaction for 30 hours at a CH_4 conversion of 40% and an H_2 yield of 20% (T=700°C, τ=10ms).

Author Contributions: Methodology, M.A., E.S., Y.B. and M.S.; investigation, K.V., V.F., A.H. and O.B.; writing—original draft preparation, M.A.; writing—review and editing, E.S., Y.B. and M.S.; supervision, V.S.; project administration, M.S.; funding acquisition, M.S. All authors have read and agreed to the published version of the manuscript.

Funding: This research was funded by Russian Science Foundation, grant number 18-73-10167.

Data Availability Statement: Not applicable.

Acknowledgments: The authors acknowledge the Shared Research Center "VTAN" of the Novosibirsk State University supported by Ministry of Science and Higher Education of the Russian Federation by agreement #075-12-2021-697 for HRTEM investigation. Authors would like to thank personally A.V. Ishchenko for carrying out HRTEM studies and A.A. Leonova for experiments of nitrogen adsorption/desorption.

Conflicts of Interest: The authors declare no conflict of interest.

References

[1] Jang, W.-J. Shim, J.-O. Kim, H.-M. Yoo, S.-Y. Roh, H.-S. A review on dry reforming of methane in aspect of catalytic properties. Catalysis Today 2019, 324, 15-26. https://doi.org/10.1016/j.cattod.2018.07.032.
[2] Aresta, M., Dibenedetto, A. Utilisation of CO2 as a chemical feedstock: opportunities and challenges. Dalton Transactions 2007, 2975-2992. https://doi.org/10.1039/B700658F.
[3] Verykios, X. E. Catalytic dry reforming of natural gas for the production of chemicals and hydrogen, International Journal of Hydrogen Energy 2003, 28, 10, 1045-1063, https://doi.org/10.1016/S0360-3199(02)00215-X.
[4] Su, B., Wang, Y., Xu, Z., Han, W, Jin, H., Wang, H. Novel ways for hydrogen production based on methane steam and dry reforming integrated with carbon capture. Energy Conversion and Management 2022, 270, 116199. https://doi.org/10.1016/j.enconman.2022.116199.
[5] Alipour, Z., Borugadda, V. B., Wang, H., Dalai, A. K. Syngas production through dry reforming: A review on catalysts and their materials, preparation methods and reactor type. Chemical Engineering Journal 2023, 452, 3, 139416. https://doi.org/10.1016/j.cej.2022.139416.
[6] Abdulrasheed, A., Jalil, A. A., Gambo, Y., Ibrahima, M., Hambali, H. U., Hamid, M.Y.S. A review on catalyst development for dry reforming of methane to syngas: Recent advances. Renewable and Sustainable Energy Reviews 2019, 108, 175–193. https://doi.org/10.1016/j.rser.2019.03.054.
[7] Yentekakis, I. V., Panagiotopoulou, P., Artemakis, G. A review of recent efforts to promote dry reforming of methane (DRM) to syngas production via bimetallic catalyst formulation. Applied Catalysis B: Environmental 2021, 296, 120210. https://doi.org/10.1016/j.apcatb.2021.120210.
[8] Rosli, S. N. A., Abidin, S. Z., Osazuwa, O. U., Fan, X., Jiao, Y. The effect of oxygen mobility/vacancy on carbon gasification in nano catalytic dry reforming of methane: A review. Journal of CO2 Utilization 2022, 63, 102109. https://doi.org/10.1016/j.jcou.2022.102109.
[9] Zhao, K., Zhang, R., Gao, Y., Lin, Y., Liu, A., Wang, X., Zheng, A., Huang, Z., Zhao, Z. High syngas selectivity and near pure hydrogen production in perovskite

Preprints (www.preprints.org) | NOT PEER-REVIEWED | Posted: 9 May 2023 doi:10.20944/preprints202305.0617.v1

oxygen carriers for chemical looping steam methane reforming. Fuel Processing Technology 2022, 236, 107398. https://doi.org/10.1016/j.fuproc.2022.107398.
[10] Li, R.-J., Zhang, J.-P., Shi, J., Li, K.-Z., Liu, H.-L., Zhu, X. Regulation of metal-support interface of Ni/CeO2 catalyst and the performance of low temperature chemical looping dry reforming of methane. Journal of Fuel Chemistry and Technology 2022, 50, 11, 1458-1470. https://doi.org/10.1016/S1872-5813(22)60032-X.
[11] K. Yu, L.-L. Lou, Sh. Liu, W. Zhou, Asymmetric Oxygen Vacancies: the Intrinsic Redox Active Sites in Metal Oxide Catalyst. Advanced Science 2020, 7, 1901970. https://doi.org/10.1002/advs.201901970.
[12] Yang, J., Hu, S., Fang, Y., Hoang, S., Li, L., Yang, W., Liang, Z., Wu, J., Hu, J., Xiao, W., Pan, C., Luo, Z., Ding, J., Zhang, L., and Guo, Y. Oxygen Vacancy Promoted O_2 Activation over Perovskite Oxide for Low-Temperature CO Oxidation. ACS Catalysis 2019, 9, 11, 9751–9763. https://doi.org/10.1021/acscatal.9b02408.
[13] Wu, L., Xie, X., Ren, H., Gao, X. A short review on nickel-based catalysts in dry reforming of methane: Influences of oxygen defects on anti-coking property. Materials Today: Proceedings 2021, 42, 153–160.
[14] Salcedo, A., Lustemberg, P. G., Rui, N., Palomino, R. M., Liu, Z., Nemsak, S., Senanayake, S. D., Rodriguez, J. A., Ganduglia-Pirovano, M. V., Irigoyen, B. Reaction Pathway for Coke-Free Methane Steam Reforming on a Ni/CeO2 Catalyst: Active Sites and the Role of Metal−Support Interactions, ACS Catalysis 2021, 11, 8327−8337. doi: 10.1021/acscatal.1c01604.
[15] McFarland, E. W., Metiu, H. Catalysis by Doped Oxides. Chemical Reviews 2013, 113, 6, 4391–4427. doi:10.1021/cr300418s.
[16] Shi, J., Li, H., Genest, A., Zhao, W., Qi, P., Wang, T., Rupprechter, G. High-performance water gas shift induced by asymmetric oxygen vacancies: Gold clusters supported by ceria-praseodymia mixed oxides. Applied Catalysis B: Environmental 2022, 301, 120789. https://doi.org/10.1016/j.apcatb.2021.120789.
[17] Vasiliades, M.A., Djinovi´c, P., Davlyatova, L.F., Pintar, A., Efstathiou, A.M. Origin and reactivity of active and inactive carbon formed during DRM over Ni/Ce0.38Zr0.62O2-δ studied by transient isotopic techniques. Catalysis Today 2018, 299, 201–211. https://doi.org/10.1016/j.cattod.2017.03.057.
[18] Puigdollers, A. R., Schlexer, P., Tosoni, S., Pacchioni, G., Increasing Oxide Reducibility: The Role of Metal/Oxide Interfaces in the Formation of Oxygen Vacancies. ACS Catalysis 2017, 7, 6493−6513. DOI: 10.1021/acscatal.7b01913.
[19] Teh, L.P., Setiabudi, H.D., Timmiati, S.N., Aziz, M.A.A., Annuar, N.H.R., Ruslan, N.N. Recent progress in ceria-based catalysts for the dry reforming of methane: A review. Chemical Engineering Science 2021, 239, 116606. https://doi.org/10.1016/j.ces.2021.116606.
[20] Salaev, M.A., Liotta, L.F., Vodyankina, O.V. Lanthanoid-containing Ni-based catalysts for dry reforming of methane: A review. International Journal of Hydrogen Energy 2022, 47, 4489-4535. https://doi.org/10.1016/j.ijhydene.2021.11.086.
[21] Makri, M.M., Vasiliades, M.A., Petallidou, K.C., Efstathiou, A.M. Effect of support composition on the origin and reactivity of carbon formed during dry reforming of methane over 5wt%Ni/Ce1−xMxO2−I (M = Zr^{4+}, Pr^{3+}) catalysts. Catalysis Today 2015, 259, 150–164. https://doi.org/10.1016/j.cattod.2015.06.010.
[22] Zhang, F., Liu, Z., Zhang, S., Akter, N., Palomino, R.M., Vovchok, D., Orozco, I., Salazar, D., Rodriguez, J.A., Llorca, J., Lee, J., Kim, D., Xu, W., Frenkel, A.I., Li, Y., Kim, T., Senanayake, S.D. In situ elucidation of the active state of Co–CeOx catalysts in the dry reforming of methane: the important role of the reducible oxide support and interactions with cobalt. ACS Catalysis 2018, 8, 3550–3560. https://doi.org/10.1021/acscatal.7b03640.
[23] Lu, M., Zhang, X., Deng, J., Kuboon, S., Faungnawakij, K., Xiao, S., Zhang, D. Coking resistant dry reforming of methane over BN–nanoceria interface-confined Ni catalysts. Catalysis Science & Technology 2020, 10, 4237–4244. https://doi.org/10.1039/d0cy00537a.

Preprints (www.preprints.org) | NOT PEER-REVIEWED | Posted: 9 May 2023 doi:10.20944/preprints202305.0617.v1

[24] Boaro, M, Colussi, S and Trovarelli, A. Ceria-Based Materials in Hydrogenation and Reforming Reactions for CO_2 Valorization. Frontiers in Chemistry 2019, 7, 28. https://doi.org/10.3389/fchem.2019.00028.
[25] Liu, B., Li, W., Song W., Liu, J. Carbonate-mediated Mars–van Krevelen mechanism for CO oxidation on cobalt-doped ceria catalysts: facet-dependence and coordination-dependence. Phys. Chem. Chem. Phys. 2018, 20, 16045-16059. https://doi.org/10.1039/c8cp01694a.
[25] Sadykov, V.A., Simonov, M.N., Mezentseva, N.V., Pavlova, S.N., Fedorova, Yu.E., Bobin, A.S., Bespalko, Yu.N., Ishchenko, A.V., Krieger, T.A., Glazneva, T.S., Larina, T.V., Cherepanova, S.V., Kaichev, V.V., Saraev, A.A., Chesalov, Y.A., Shmakov, A.N., Roger, A-C., Adamski, A. Ni-loaded nanocrystalline ceria-zirconia solid solutions prepared via modified Pechini route as stable to coking catalysts of CH_4 dry reforming. Open Chem 2016, 14, 363–376. https://doi.org/10.1515/chem-2016-0039.
[26] Smirnova, M.Yu., Pavlova, S.N., Krieger, T.A., Bespalko, Yu.N., Anikeev, V.I., Chesalov, Yu.A., Kaichev, V.V., Mezentseva, N.V., Sadykov, V.A. The synthesis of Ce1–xZrxO2 oxides in supercritical alcohols and catalysts for carbon dioxide reforming of methane on their basis. Russian Journal of Physical Chemistry B 2017, 12, 15–28. https://doi.org/10.1134/S1990793117080103.
[27] Vasiliades, M.A., Makri, M.M., Djinovic´, P., Erjavec, B., Pintar, A., Efstathiou, A.M. Dry reforming of methane over 5 wt% Ni/Ce1-xPrxO2-catalysts: Performance and characterisation of active and inactive carbon by transient isotopic techniques. Applied Catalysis B: Environmental 2016, 197, 168–183. https://doi.org/10.1016/j.apcatb.2016.03.012.
[28] Sinev, M.Yu., Graham, G.W., Haack, L.P., Shelef, M. Kinetic and structural studies of oxygen availability of the mixed oxides $Pr_{1-x}M_xO_y$ (M = Ce, Zr). J. Mater. Res. 1996, 11, 1960-1971. https://doi.org/10.1557/JMR.1996.0247.
[29] Niu, G., Zoellner, M.H., Schroeder, T., Schaefer, A., Jhang, J.H., Zielasek, V., B¨aumer, M., Wilkens, H., Wollschlager, J., Olbrich, R., Lammers, C., Reichling, M. Controlling the physics and chemistry of binary and ternary praseodymium and cerium oxide systems. Phys. Chem. Chem. Phys. 2015, 17, 24513–24540. https://doi.org/10.1039/C5CP02283E.
[30] Kambolis, A., Matralis, H., Trovarelli, A., Papadopoulou, Ch. Ni/CeO2-ZrO2 catalysts for the dry reforming of methane. Appl. Catal. A 2010, 377, 16–26. https://doi.org/10.1016/j.apcata.2010.01.013.
[31] Hirano, M., Hirai, K. Effect of hydrolysis conditions on the direct formation of nanoparticles of ceria–zirconia solid solutions from acidic aqueous solutions. J. Nanoparticle Res. 2003, 5, 147–156. https://doi.org/10.1023/A:1024482824561.
[32] Pradeep, E., Habu, T., Tooriyama, H., Ohtani, M., Kobiro K. Ultra-simple synthetic approach to the fabrication of CeO2–ZrO2 mixed nanoparticles into homogeneous, domain, and core–shell structures in mesoporous spherical morphologies using supercritical alcohols. J. Supercrit. Fluids 2015, 97, 217-223. https://doi.org/10.1016/j.supflu.2014.12.004.
[33] Montoya, J.A., Romero-Pascual, E., Gimon, C., Del Angel, P., Monzón, A. Methane reforming with CO2 over Ni/ZrO2-CeO2 catalysts prepared by sol-gel. Catal. Today 2000, 63, 71–85. https://doi.org/10.1016/S0920-5861(00)00447-8.
[34] Luisetto, I., Tuti, S., Romano, C., Boaro, M., Di Bartolomeo, E., Kesavan, J.K., Kumar, S.S., Selvakumar, K. Dry reforming of methane over Ni supported on doped CeO2: New insight on the role of dopants for CO_2 activation. J. CO2 Util. 2019, 30, 63–78. https://doi.org/10.1016/j.jcou.2019.01.006.
[35] Kuznetsova, T.G., Sadykov, V.A., Moroz, E.M., Trukhan, S.N., Paukshtis, E.A., Kolomiichuk, V.N., Burgina, E.B., Zaikovskii, V.I., Fedotov, M.A., Lunin, V.V., Kemnitz, E. Preparation of Ce-Zr-O composites by a polymerized complex method. Stud. Surf. Sci. Catal 2002, 143, 659–667. https://doi.org/10.1016/S0167-2991(00)80708-9.

Preprints (www.preprints.org) | NOT PEER-REVIEWED | Posted: 9 May 2023 doi:10.20944/preprints202305.0617.v1

[36] Basile, F., Mafessanti, R., Fasolini, A., Fornasari, G., Lombardi, E., Vaccari A. Effect of synthetic method on CeZr support and catalytic activity of related Rh catalyst in the oxidative reforming reaction. J. Eur. Ceram 2019, 39, 41–52. https://doi.org/10.1016/j.jeurceramsoc.2018.01.047.
[37] Cai, W., Dong, J., Chen, Q., Xu, T., Zhai, S., Liu, X., Cui, L., Zhang S. One-pot microwave-assisted synthesis of Cu-Ce0.8Zr0.2O2 with flower-like morphology: Enhanced stability for ethanol dry reforming. Adv Powder Technol 2020, 31, 3874–3881. https://doi.org/10.1016/j.apt.2020.07.032.
[38] Manjunatha, S., Dharmaprakash, M.S., Thermal stability, optical and Photoluminescence properties of spherical CexZr1−xO2 (x = 0.05) crystalline blue-emitting nanophosphors synthesized by microwave method. Mater. Res. Express, 2018, 5, 035043. https://doi.org/10.1088/2053-1591/aab518.
[39] Guo, J., Xin, X., Zhang, X., Zhang, S. Ultrasonic-induced synthesis of high surface area colloids CeO2–ZrO2. J Nanopart Res 2009, 11, 737–741. https://doi.org/10.1007/s11051-008-9504-y.
[40] Khani, Y., Bahadoran, F., Shariatinia, Z., Varmazyari, M., Safari, N. Synthesis of highly efficient and stable Ni/CexZr1-xGdxO4 and Ni/X-Al2O3 (X = Ce, Zr, Gd, Ce-Zr-Gd) nanocatalysts applied in methane reforming reactions. Ceram. Int. 2020, 46, 25122–25135. https://doi.org/10.1016/j.ceramint.2020.06.299.
[41] Guo, T., Du, J., Wu, J., Li, J. Enhanced properties of solid solution (CeZr)O2 modified with metal oxides for catalytic oxidation of low-concentration methane. Chin. J. Chem. Eng. 2017, 25, 187–192. https://doi.org/10.1016/j.cjche.2016.07.016.
[42] Lovell, E., Horlyck, J., Scott, J., Amal, R. Flame spray pyrolysis-designed silica/ceria-zirconia supports for the carbon dioxide reforming of methane. Appl. Catal. 2017, 546, 47–57. https://doi.org/10.1016/j.apcata.2017.08.002.
[43] Veriansyah, B., Park, H., Kim, J.D., Min, B.K., Shin, Y.H., Lee, Y.W., Kim, J. Characterization of surface-modified ceria oxide nanoparticles synthesized continuously in supercritical methanol. J Supercrit Fluids 2009, 50, 283-291. https://doi.org/10.1016/j.supflu.2009.06.007.
[44] Lustemberg, P.G., Mao, Z., Salcedo, A., Irigoyen, B, Ganduglia-Pirovano, M.V., Campbell, C.T. Nature of the active sites on Ni/CeO2 catalysts for methane conversions. ACS Catal. 2021, 11, 10604−10613. https://doi.org/10.1021/acscatal.1c02154.
[45] Li, M., van Veen, A.C. Tuning the catalytic performance of Ni-catalysed dry reforming of methane and carbon deposition via Ni-CeO2-x interaction. Applied Catalysis B: Environmental 2018, 237, 641–648. https://doi.org/10.1016/j.apcatb.2018.06.032.
[46] Anchieta, C.G., Assaf, E.M., Assaf, J.M. Syngas production by methane tri-reforming: Effect of Ni/CeO2 synthesis method on oxygen vacancies and coke formation. Journal of CO2 Utilization 2022, 56, 101853. https://doi.org/10.1016/j.jcou.2021.101853.
[47] Lyu, Y., Jocz, J.N., Xu, R., Stavitski, E., Sievers, C. Nickel speciation and methane dry reforming performance of Ni/CexZr1-xO2 prepared by different synthesis methods. ACS Catal. 2020, 10, 11235-11252. https://doi.org/10.1021/acscatal.0c02426.
[48] Bespalko, Y., Smal, E., Simonov, M., Valeev, K., Fedorova, V., Krieger, T., Cherepanova, S., Ishchenko, A., Rogov, V., Sadykov, V. Novel Ni/Ce(Ti)ZrO2 catalysts for methane dry reforming prepared in supercritical alcohol media. Energies 2020, 13, 3365. https://doi.org/10.3390/en13133365.
[49] Simonov, M., Bespalko, Y., Smal, E., Valeev, K., Fedorova, V., Krieger, T., Sadykov, V. Nickel-containing ceria-zirconia doped with Ti and Nb. Effect of support composition and preparation method on catalytic activity in methane dry reforming. Nanomaterials 2020, 10, 1281. https://doi.org/10.3390/nano10071281.
[50] Rietveld, H.M. A profile refinement method for nuclear and magnetic structures. Journal of Applied Crystallography, 1969, 2, 65-71. https://doi.org/10.1107/S0021889869006558.

Preprints (www.preprints.org) | NOT PEER-REVIEWED | Posted: 9 May 2023 doi:10.20944/preprints202305.0617.v1

[51] Ballauri, S., Sartoretti, E., Novara, C., Giorgis, F., Piumetti, M., Fino, D., Russo, N., Bensaid, S. Wide range temperature stability of palladium on ceria-praseodymia catalysts for complete methane oxidation. Catalysis Today 2022, 390-391, 185–197. https://doi.org/10.1016/j.cattod.2021.11.035.
[52] Makri, M.M., Vasiliades, M.A., Petallidou, K.C., Efstathiou, A.M. Effect of support composition on the origin and reactivity of carbon formed during dry reforming of methane over 5wt%Ni/Ce1−xMxO2−δ (M = Zr4+, Pr3+) catalysts. Catal. Today 2016, 259, 150–164. https://doi.org/10.1016/j.cattod.2015.06.010.
[53] Rajendran, M., Mallick, K.K., Bhattacharya, A.K., Combustion synthesis, powder characteristics and crystal structure of phases in Ce–Pr–O system. J. Mater. Sci. 1998, 33, 5001–5006. https://doi.org/10.1023/A:1004459024431.
[54] Iglesias, I., Baronetti, G., Marino, F. Ni/Ce0.95M0.05O2-d (M = Zr, Pr, La) for methane steam reforming at mild conditions. Int J Hydrogen Energy 2017, 42, 29735-29744. https://doi.org/10.1016/j.ijhydene.2017.09.176.
[55] Jalowiecki-Duhamel, L., Zarrou, H., D'Huysser, A. Hydrogen production at low temperature from methane on cerium and nickel based mixed oxides. Int J Hydrogen Energy 2008, 33, 5527-5534. https://doi.org/10.1016/j.ijhydene.2008.07.031.
[56] Takeguchi, T., Furukawa, S.N., Inoue, M. Hydrogen spillover from NiO to the large surface area CeO2-ZrO2 solid solutions and activity of the NiO/CeO2-ZrO2 catalysts for partial oxidation of methane. J Catal 2001, 202, 14-24. https://doi.org/10.1006/jcat.2001.3249.
[57] Smal, E., Bespalko, Y., Arapova, M., Fedorova, V., Valeev, K., Eremeev, N., Sadovskaya, E., Krieger, T., Glazneva, T., Sadykov, V., Simonov, M. Carbon formation during methane dry reforming over Ni-containing ceria-zirconia catalysts. Nanomaterials 2022, 12, 3676. https://doi.org/10.3390/nano12203676.